Unveiling the anatomy of Termination 3 using water and air isotopes in the Dome C ice core, East Antarctica

Camille Bréant, Amaelle Landais, Anais Orsi, Patricia Martinerie, Thomas Extier, Frédéric Prié, Barbara Stenni, Jean Jouzel, Valérie Masson-Delmotte, Markus Leuenberger

Unveiling the anatomy of Termination 3 using water and air isotopes in the Dome C ice core, East Antarctica

Camille Bréant[1,2], Amaëlle Landais[1,*], Anaïs Orsi[1], Patricia Martinerie[2], Thomas Extier[1], Frédéric Prié[1], Barbara Stenni[3], Jean Jouzel[1], Valérie Masson-Delmotte[1] and Markus Leuenberger[4]

[1] Laboratoire des Sciences du Climat et de l'Environnement, LSCE/IPSL, CEA-CNRS-UVSQ, Université Paris-Saclay, Gif-sur-Yvette, France

[2] Univ. Grenoble Alpes, CNRS, IRD, Grenoble INP, IGE, Grenoble, 38000, France

[3] Department of Environmental Sciences, Informatics and Statistics, University Ca' Foscari of Venice, Venice, Italy

[4] Climate and Environmental Physics, Physics Institute and Oeschger Center for Climate Research, University of Bern, Sidlerstrasse, 5, 3012 Bern, Switzerland

[*] corresponding author from February 2019: amaelle.landais@lsce.ipsl.fr

Abstract

Each glacial – interglacial transition of the Quaternary occurs in a different orbital context leading to various timing for the deglaciation and sequence of high vs low latitudes events. Termination 3, 250 kiloyears before present (ka), is an unusual deglaciation in the context of the last 9 deglaciations recorded in the old EPICA Dome C (EDC) Antarctic ice core: it exhibits a three-phase sequence, two warming phases separated by a small cooling, the last phase suggesting a particularly rapid temperature increase. We present here new high resolution $\delta^{15}N$ and deuterium excess (d-excess) data from the EDC ice core to provide a detailed temperature change estimate during this termination. Then, we combined the δD and $\delta^{18}O$ to discuss the relationship between high and low latitude changes through the d-excess. We also provide the high vs low latitude sequence of events over this deglaciation without chronological uncertainty using low latitude ice core proxies. In agreement with previous studies based on speleothem analyses, we show that the first phase of Termination 3 (256 to 249 ka) is associated with small Heinrich like events linked to changes in ITCZ position, monsoon activity and teleconnections with Antarctica. In a context of minimum Northern Hemisphere insolation,

this leads to a rather strong Antarctic warming, as observed in the $\delta^{15}N$ record in contrast to the relatively small δD increase. The second warming phase occurs during the rise of the Northern hemisphere insolation, with a large Heinrich like event leading to the characteristic Antarctic warming observed in the $\delta^{15}N$ and δD increase as for the more recent terminations.

Keywords

Termination 3, deglaciations, ice core, water and air isotopes, Antarctic temperature, firn densification model, bipolar seesaw, Heinrich like events

1- Introduction

The climate of the Quaternary is characterized by the succession of glacial and interglacial periods, with a detailed description of their characteristics thanks to a diversity of proxy records from oceanic, terrestrial and glacial archives, and dating methods (Spratt & Lisiecki 2016; Jouzel et al. 2007; Tzedakis et al. 2017). The occurrence of glacial and interglacial periods is generally attributed to the driving effect of changes in the seasonal and latitudinal distribution of incoming solar radiation, due to changes in the Earth's astronomical characteristics (Milankovitch, 1941), as well as key Earth system feedbacks, involving ice sheet and carbon cycle dynamics (Paillard & Parrenin 2004).

The exact mechanisms at play during glacial terminations remain however elusive, and explanations for the timing of terminations, the different magnitudes of glacial-interglacial transitions, and the interplay between multi-millennial trends and abrupt events are still incomplete. The accurate documentation of multiple terminations, taking place under different orbital contexts, is one key line of evidence (Yin and Berger, 2012; PAGES, 2016; Tzedakis et al., 2017). The important role of obliquity is directly visible on the 40 kiloyears (hereafter ka) periodicity of glacial – interglacial cycles occurring before the mid-Pleistocene transition and can also be dominant in the younger terminations (Huybers, 2007). In parallel, a recent study using East Asian speleothems showed that deglaciations of the last 650 ka occur every 4 or 5 precession cycles, confirming the important role of precession (Cheng et al.,

2016). The unfolding (or not) of a deglaciation during a precession cycle has been suggested to be related to the glacial state, such as the initial ice volume (Paillard et al., 1998), or integrated summer insolation (Tzedakis et al., 2017). The concentration of atmospheric greenhouse gases also plays a major role during deglaciations. Several studies have shown, within age scale uncertainties, that atmospheric CO_2 concentration and East Antarctic temperature started to increase synchronously at the beginning of the last two deglaciations (Pedro et al., 2012; Landais et al., 2013; Parrenin et al., 2013). The amplitude of simulated global temperature changes over deglaciations has been shown to depend jointly on the amplitude of CO_2 concentration increase and insolation, namely obliquity for the Southern Hemisphere and precession for the Northern Hemisphere (Yin and Berger, 2012).

The Antarctic EPICA Dome C (EDC) ice core provides very high resolution records encompassing changes in local climate (with a resolution of 20 to 50 years back to 430 ka) as well as changes in atmospheric composition and greenhouse gases concentrations of the last 9 terminations (EPICA Community Members, 2004; Jouzel et al., 2007; Loulergue et al., 2008; Lüthi et al., 2008; Bereiter et al., 2015). Together with the sea level record obtained from marine sediments (e.g. Röhling et al., 2014; Spratt and Lisiecki, 2016), the δD record from the EDC ice core shows that the last 5 terminations (i.e. over the last 430 ka) are generally of higher amplitude than the terminations over the period 800 – 430 ka. Each termination still displays different characteristics (amplitude, rate of change) that were discussed in previous studies (Röthlisberger et al., 2008; PAGES, 2016). In this context, Termination 3 seems associated with the most rapid temperature increase (increase of EDC δD at 14.8 ‰.ka^{-1} for the period 251.5 to 247.8 ka – Figure 1) making it a pertinent benchmark for the study of climate change on relatively short timescales.

Marine records show that terminations of at least the last 500 ka are systematically associated with the occurrence of iceberg discharges from the Laurentide ice sheet recorded as occurrence of Heinrich like events in the IRD (Ice Rafted Debris characterized by a large amount of detrital quartz in the sediment) in Atlantic marine cores (McManus et al., 1999; Hodell et al., 2008). In parallel, East Asian speleothems highlight systematic Weak Monsoon Intervals (WMI) occurring during the

terminations synchronously with Heinrich like events and a rise in Northern Hemisphere summer insolation (Cheng et al., 2009; 2016). Mechanistic links exist between Heinrich like events and WMI: Heinrich like events are occurring over the same millennial periods as southward shifts of atmospheric circulation in the Northern Hemisphere and in particular with southward shifts of tropical rain belts (Chiang and Bitz, 2005). The Heinrich like events and associated lower latitudes climate changes are hence fully embedded in the dynamic of terminations (e.g. Wolff et al., 2009; Denton et al., 2010). Again, Termination 3 stands out being associated with 3 IRD peaks and 3 WMI while other terminations over the last 450 ka are associated with only 1 or 2 IRD peaks (Jiang et al., 2010; Obrochta et al., 2014; Figure 1). The unusual sequence observed over Termination 3 between millennial events and polar temperature increase makes the study of Termination 3 key to understand the interactions between millennial events (Heinrich Stadials, WMI) and orbital change (long term increase in CO_2 and polar temperature).

Only few studies provided up to centennial resolution data for Termination 3, all of them highlighting millennial scale variability during the end of marine isotopic stage 8 and Termination 3, both in the Northern and in the Southern Hemispheres (i.e. between ~260 and 245 ka) (Pahnke et al., 2003; Cheng et al., 2009; Jiang et al., 2010; Pérez-Mejías et al., 2017). In Antarctic deep ice cores, two warming phases have been identified within Termination 3 (e.g. Watanabe et al., 2003; Röthlisberger et al., 2008), the first one being associated with a relatively slow δD increase (5.18 ‰.ka^{-1}), interpreted to reflect a gradual warming, before the fastest δD rise interpreted to reflect a fast warming.

Here, we focus on Termination 3 using new datasets from the EDC ice core. We combine water isotopes (published δD and new δ^{18}O data) with new δ^{15}N of N_2 trapped in air bubbles, thereafter δ^{15}N. The combination of water isotopes, δD and δ^{18}O already published over the last 2 deglaciations at Dome C (Stenni et al., 2001, 2010; Masson-Delmotte et al., 2010), can indeed be very useful to discuss the relationship between local (δ^{18}O and δD at first order) and lower latitudes climatic changes (deuterium excess or d-excess defined as δD - 8*δ^{18}O) (e.g. Vimeux et al., 1999; Uemura et al., 2018). δ^{15}N is a proxy of firn processes driven by changes in local accumulation and temperature

(Severinghaus et al. 1998) providing an indicator of Antarctic climate change in the gas phase of the ice core records (Caillon et al., 2003; Landais et al., 2013). We briefly describe our methods, and discuss our results, including the reconstruction of site and source temperatures from water stable isotopes, and the drivers of $\delta^{15}N$ at EDC over Termination 3. We finally compare to previous records from other archives (marine sediment cores and speleothems) and discuss the sequence of events encompassing changes in Antarctic and global climate over Termination 3.

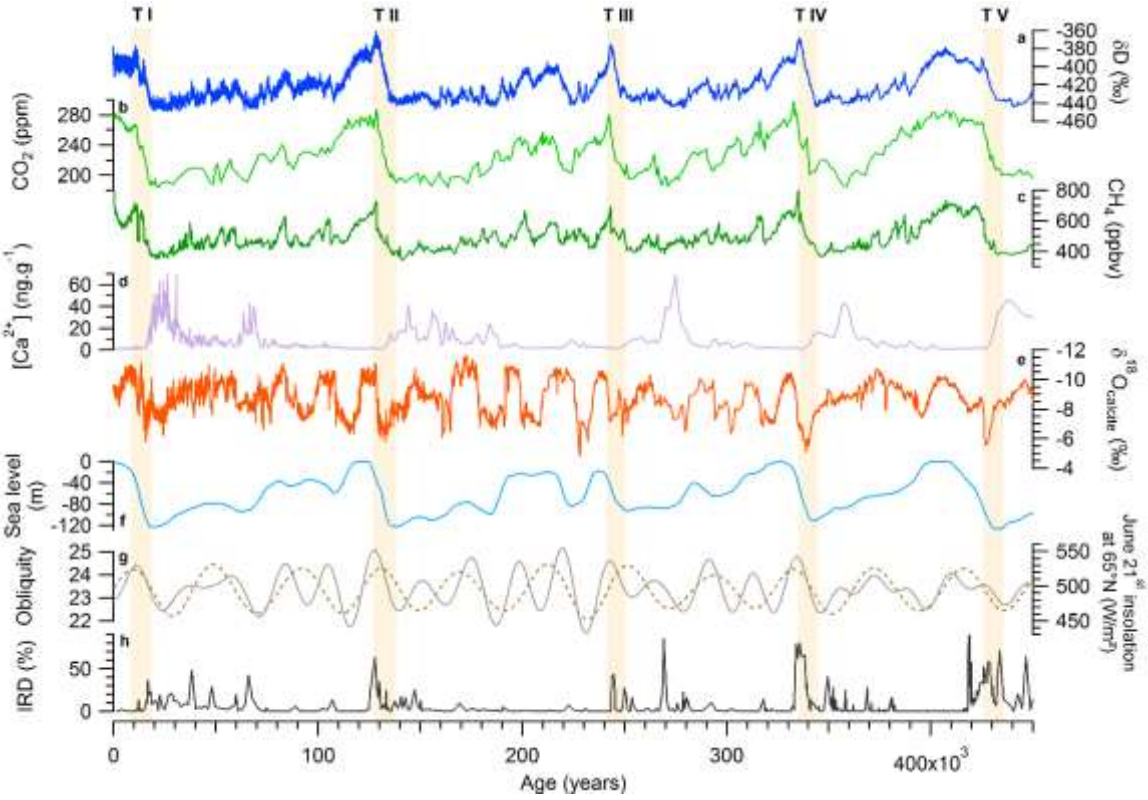

Figure 1: *Climatic variations over the last 450 ka. a: δD record from EDC (Jouzel et al., 2007). b: Antarctic CO_2 from EDC and Vostok (Lüthi et al., 2008). c: East Antarctic CH_4 record (Loulergue et al., 2008) d: Ca^{2+} concentration in the EDC ice core (Lambert et al., 2012). e: $\delta^{18}O_{calcite}$ from East Asian speleothems (Cheng et al., 2016). f: Global sea level change estimate (Bintanja et al., 2005). g: June 21st insolation at 65°N in solid line and obliquity in dotted line (Laskar et al., 2004). h: IRD percentage at site ODP980 (McManus et al., 1999). The timing of Termination 5 (TV) to Termination 1 (TI) is indicated by yellow bars. The 4 upper records are issued from the same ice core, hence with a maximum relative uncertainty of 1 ka on the chronology. On opposite, the 4 lower curves are all on their respective timescales (absolute timescale for obliquity and precession; timescale of each archive for the others) so that uncertainties of up to 6 ka can be attached to the comparison of the different records.*

2- New data

2-1- EPICA Dome C (EDC) $\delta^{18}O$ and d-excess

Water $\delta^{18}O$ measurements of the Dome C ice core were performed along 55 cm samples at the Department of Earth Sciences of University of Parma and at the Department of Geological, Environmental and Marine Sciences of University of Trieste using a CO_2 / water equilibration method (Meyer et al., 2000). These new measurements complete the 800 ka δD records of the EDC ice core previously obtained at Laboratoire des Sciences du Climat et de l'Environnement and published in (Jouzel et al., 2007). Home water standards were exchanged between the three institutes during the measurement period to ensure the proper comparison of the δD and $\delta^{18}O$ data series. d-excess was then calculated from the combined measurements of δD and $\delta^{18}O$ with a resulting accuracy of 1‰.

The δD and d-excess series presented on the section 3 cover the time period 230 to 270 ka with an uncertainty of about 3 ka on the AICC2012 timescale (Bazin et al., 2013). This period corresponds to the depth range 2232 to 2381 m and extends the EDC $\delta^{18}O$ and d-excess records over the last 140 ka (Stenni et al., 2010).

As already noted, the δD record shows a two-step increase for Termination 3: a first increase of 15‰ occurs from 253 to 249 ka (phase III-a, Figure 2). The same pattern was also observed on the other deep ice cores covering Termination 3 on which water isotopes have been measured (SOM – Figure S1). d-excess shows a parallel increase to δD over phase III-a. d-excess and δD are then anti-correlated during the major δD increase of Termination 3 between 248 and 243 ka (phase III-b, Figure 2). Finally, d-excess reaches a maximum during the glacial inception, i.e. when δD is decreasing from 243 to 230 ka (Figure 2). This d-excess signal during glacial inceptions is a classical pattern also observed for other glacial inceptions in Antarctic ice cores (Vimeux et al., 1999; Stenni et al., 2010; Uemura et al., 2018): d-excess increases while δD decreases.

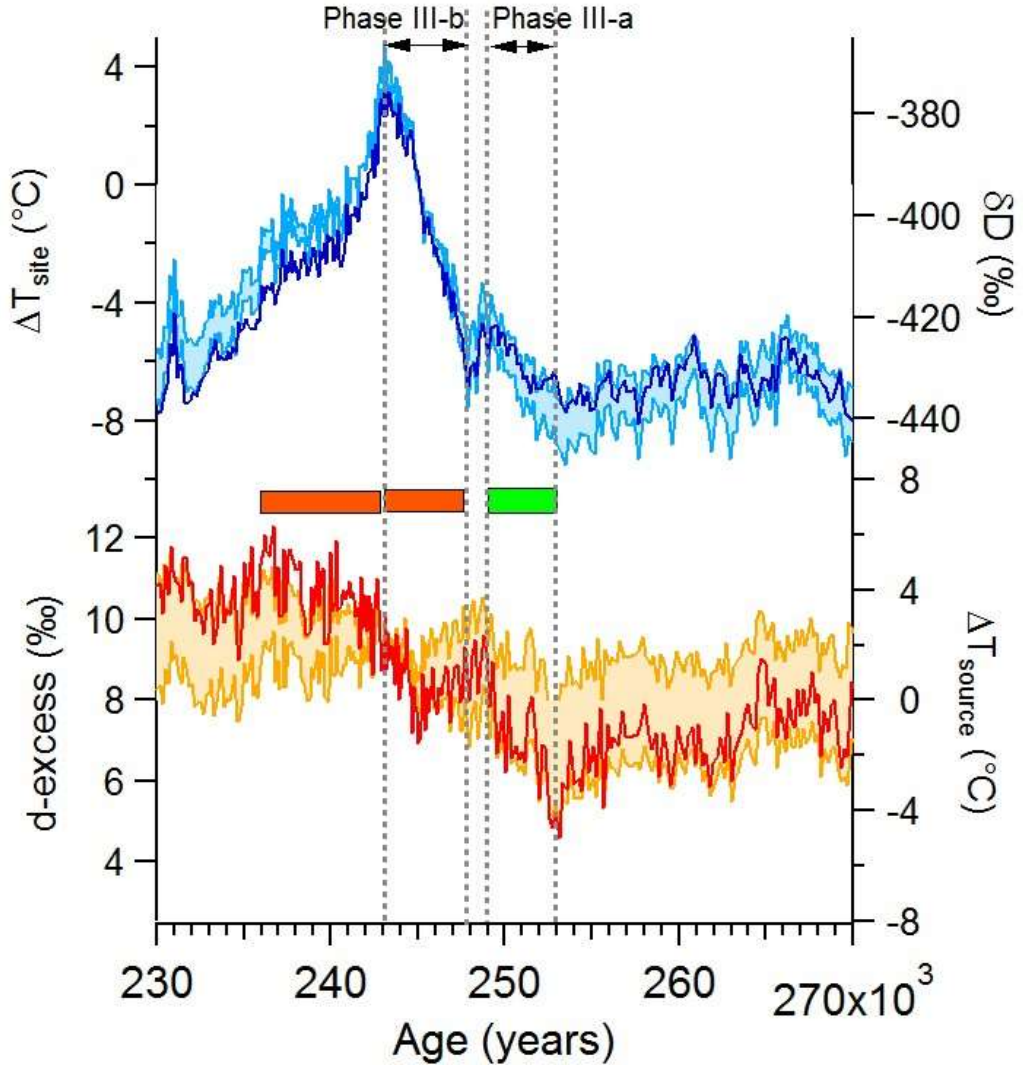

Figure 2**:** *δD (in dark blue) and d-excess (in red) measurements on Dome C ice core with highlights on the phases of correlation (green rectangle) and anti-correlation (red rectangles) between these two proxies over the Termination 3. The ΔT_{site} and ΔT_{source} reconstructions within their uncertainty ranges are displayed in shaded areas. The vertical shaded lines display the limits of phase III-a and phase III-b.*

2-2- EDC $\delta^{15}N$

Three series of measurements of $\delta^{15}N$ of N_2 have been performed along Termination 3 on the EDC ice core (Figure 3):

1- 50 duplicate samples (2262 to 2352 m depth) were measured in 2008 at Princeton University using a semi-automated wet extraction line with associated uncertainty of 7 ppm (Dreyfus et al., 2010).

2- 48 duplicate samples (2268 to 2348 m depth) were measured in 2013 at LSCE using a semi-automated wet extraction line with associated uncertainty of 10 ppm (method in Capron et al., 2010).

3- 172 duplicate samples (1904 to 2580 m depth) were measured in 2015-2016 at LSCE using the same semi-automated wet extraction line and similar associated uncertainty of 10 ppm.

$\delta^{15}N$ measurements are expressed with respect to $\delta^{15}N$ of atmospheric air, with expected similar values at Princeton University and at LSCE. Still, an average shift of + 0.007 ‰ has been found in the original Princeton values compared to the LSCE data. The source of this offset is unknown. We thus follow the correction of Dreyfus et al. (2010) and subtracted 0.007 ‰ from all Princeton data in the set of data presented here.

As already shown in Dreyfus et al. (2010), $\delta^{15}N$ record shows a clear and strong increase from 2350 m to 2310 m depth probably corresponding to Termination 3 according to the AICC2012 gas age timescale for EDC (Figure 3). After a $\delta^{15}N$ maximum at 2308 m probably associated with the end of Termination 3, $\delta^{15}N$ shows a clear decrease from 2308 to 2250 m. Deeper in the core, the $\delta^{15}N$ record is more scattered, showing a general decreasing tendency from 2580 m to 2350 m with some fluctuations over the depth range 2480 m to 2350 m (Figure 3).

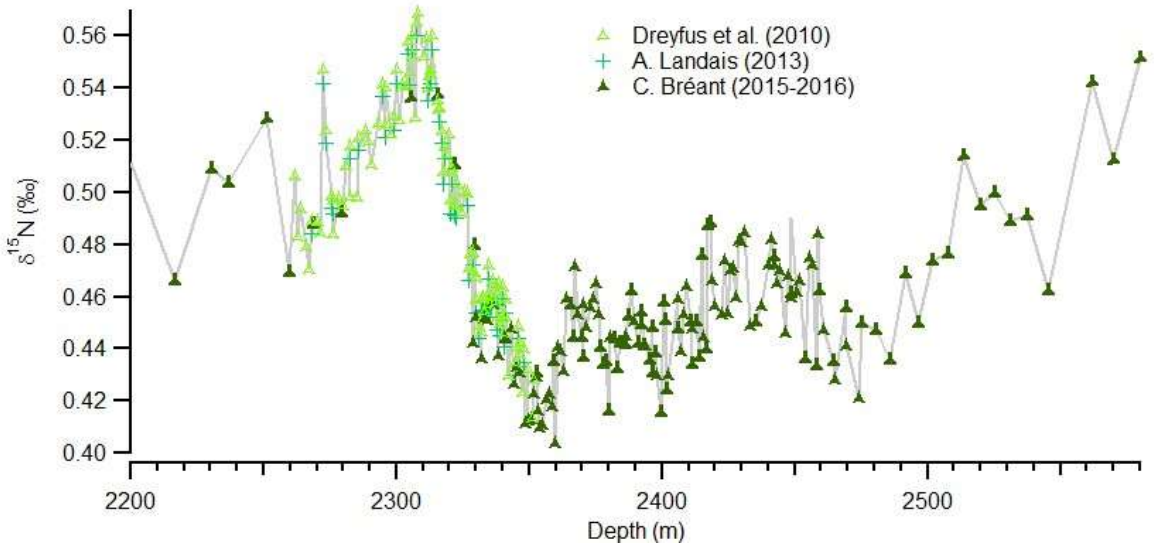

Figure 3: *$\delta^{15}N$ data for Termination 3 of Dome C ice core using the correction for data measured in Princeton vs LSCE proposed by Dreyfus et al. (2010).*

The main $\delta^{15}N$ increase corresponding to Termination 3 on the EDC core was also observed on the Vostok $\delta^{40}Ar$ data over the same termination (Caillon et al., 2003), $\delta^{40}Ar$ being assumed to be related to physical fractionations in the firn before bubble enclosure as for $\delta^{15}N$ (see next section). Finally, $\delta^{15}N$ deglacial increase of ~0.15‰ was also clearly observed over the other terminations at EDC (Dreyfus et al., 2010, SOM – Figures S2 and S3).

3- Interpretation of the d-excess and $\delta^{15}N$ signals

3-1- Interpretation of water stable isotopes: site and source temperature

Records of d-excess in Antarctic polar ice cores have classically been used to infer changes in moisture sources / evaporation conditions following the studies of Vimeux et al. (1999), Stenni et al. (2001), Vimeux et al. (2001), Masson-Delmotte et al. (2010), Markle et al. (2016) and Uemura et al. (2018). In surface water vapour, at synoptic timescales, d-excess variations are mainly influenced by variations in relative humidity controlling the relative influence of kinetic and equilibrium effects (Merlivat and Jouzel, 1979; Gat et al., 1991). This influence is however muted when looking at the d-excess evolution in polar regions and on longer timescales. Moreover d-excess is strongly modified during distillation from the source to the polar precipitation regions through two effects: (1) the dependence of equilibrium fractionation coefficient at condensation with temperature and (2) the decrease of the slope δD vs $\delta^{18}O$ when both δD and $\delta^{18}O$ decrease toward very negative values (e.g. Jouzel and Merlivat, 1984; Touzeau et al., 2016). This effect becomes predominant in very cold regions of East Antarctica, for extremely low δD and $\delta^{18}O$. In these circumstances, local cooling leads to a d-excess increase not linked to moisture source characteristics (Uemura et al., 2012). Alternative definitions of d-excess using a logarithm formulation have thus been proposed to circumvent this site temperature signal (e.g. Uemura et al., 2012; Markle et al., 2016; Dütsch et al., 2017). However, the $\ln(\delta D+1)$ vs $\ln(\delta^{18}O+1)$ slope is not as constant as the $\delta^{18}O$ vs δD slope for large $\delta^{18}O$ – δD ranges, hence leading to variable slope as a function of $\delta^{18}O$ values when defining the excess with a logarithm

definition. Here, we made the choice to show the d-excess curves keeping the classical d-excess definition. This choice of definition does not affect the reconstructions displayed below.

Following earlier studies of EDC d-excess, the combination of δD and d-excess can be used to reconstruct the local temperature (T_{site}) and the moisture source temperature (T_{source}). The moisture sources for precipitation at Dome C are located mainly in the temperate area of the Indian ocean (Masson-Delmotte et al., 2010). Here, we use the values for the T_{site} and T_{source} reconstructions for the EDC site given by Stenni et al. (2010) based on the use of a theoretical, mixed cloud isotopic model and the assumption that relative humidity is constant:

$$\Delta T_{site} = 0.16 \times \Delta\delta D_{corr} + 0.44 \times \Delta d\text{-}excess_{corr} \quad (1)$$

$$\Delta T_{source} = 0.06 \times \Delta\delta D_{corr} + 0.93 \times \Delta d\text{-}excess_{corr} \quad (2)$$

The Δ symbol stands for the difference at each level between the measured or reconstructed parameter and the average of this parameter for the recent period (we performed the average over the last 2000 years for the reference to "the recent period"). ΔdD_{corr} and $\Delta d\text{-}excess_{corr}$ were calculated following Jouzel et al. (2003) using the $\delta^{18}O_{sea\ water}$ obtained in Bintanja et al. (2005) synchronized on EDC timescale (Parrenin et al., 2007):

$$\delta D_{corr} = \left[\delta D - 8 \times \delta^{18}O_{sea\ water} \times \left(1 + \frac{\delta D}{1000}\right)\right] \div \left[1 + 8 \times \left(\frac{\delta^{18}O_{sea\ water}}{1000}\right)\right] \quad (3)$$

$$\delta^{18}O_{corr} = \left[\delta^{18}O - \delta^{18}O_{sea\ water} \times \left(1 + \frac{\delta^{18}O}{1000}\right)\right] \div \left[1 + \left(\frac{\delta^{18}O_{sea\ water}}{1000}\right)\right] \quad (4)$$

$$\Delta\delta D_{corr} = \delta D_{corr} - \delta D_{average} \quad (5)$$

$$\Delta\delta^{18}O_{corr} = \delta^{18}O_{corr} - \delta^{18}O_{average} \quad (6)$$

$$\Delta d - excess_{corr} = \Delta\delta D_{corr} - 8 \times \Delta\delta^{18}O_{corr} \quad (7)$$

These temperature reconstructions are based on the use of a mixed cloud isotopic model (Ciais and Jouzel, 1994) describing the evolution of water isotopic composition along a trajectory toward Antarctica and run over a large range of T_{site} and T_{source}. Different tunings of this model can however lead to significant variations in the coefficients of equations (1) and (2). Alternative reconstructions

have thus been proposed (e.g. Uemura et al., 2012 for a complete study) enabling one to provide the uncertainty range to the T_{site} and T_{source} reconstructions displayed on Figure 2. These alternative reconstructions do not affect the shape of the reconstructed T_{site} and T_{source} variations but the amplitudes of variations over Termination 3 are significantly affected, especially for the T_{source} reconstruction (Figure 2).

The T_{site} and T_{source} reconstructions for Dome C are presented on Figure 2. While the evolution of T_{site} is mainly parallel to the δD evolution and share many similarities with it, some differences are observed. Over phase III-a, T_{site} displays an increase equivalent to 2/5 of the main T_{site} increase over Termination 3 occurring during phase III-b. Over the same period (phase III-a, 253 to 249 ka), δD only shows an increase of 1/4 of the main δD increase over phase III-b. The fact that the increase of EDC δD over phase 1 of Termination 3 is relatively smaller than the corresponding T_{site} increase is probably because δD is not only sensitive to the local temperature but rather to the temperature gradient between the evaporative site and the precipitation site (i.e. between the first and final point of the distillation trajectory). The T_{source} reconstruction based on d-excess data shows an increase over phase III-a on Termination 3, in parallel to the T_{site} increase (Figure 2). Since both T_{site} and T_{source} increase by similar amplitude, we expect that the result is the small δD signal observed on the EDC record. Over phase III-b, T_{source} is not varying much (slight decrease) so that the dynamic of δD increase is directly reflected in the T_{site} increase. T_{source} evolution is very different from the T_{site} evolution over glacial inception: it follows the d-excess signal which remains at a relatively high level. This signal was already largely discussed in Vimeux et al. (1999) and following studies: it reflects the fact that the temperature of moisture source remains high during glacial inception favoring evaporation in temperate latitudes and hence significant transport of moisture toward polar area to contribute to the growing of glacial ice sheets.

The T_{site} and δD signals exhibit some differences during the glacial inception with the T_{site} signal decreasing less rapidly than the δD signal. While this relatively slower decrease of T_{site} compared to δD is also observed for other glacial inceptions and on the Vostok and Dome C ice cores (Vimeux et al.,

2001; Stenni et al., 2010; SOM – Figure S1), the differences in the T_{site} vs δD behaviours observed over Termination 3 is less obvious for the other terminations. Finally, note that the δD vs T_{site} differences are much less visible at the Dome F site, the δD signal at Dome F sharing more variability with the T_{site} signal than at Dome C or Vostok (SOM – Table T1).

3-2- Interpretation of the $\delta^{15}N$ signal

In a previous study (Bréant et al., 2017), we summarized the different possible influences on the $\delta^{15}N$ in Antarctic ice core. $\delta^{15}N$ is directly related to the depth of the firn diffusive zone through gravitational fractionation as $\delta^{15}N_{grav} = gz/RT$ at first order approximation with z the depth of the diffusive zone, g the gravity acceleration constant, R the gas constant and T the mean temperature. Note that a second order thermal effect is also expected in Antarctica when temperature gradients occur in the firn following the equation $\delta^{15}N_{therm} = \Omega \times \Delta T$ with Ω the thermal fractionation coefficient for stable isotopes of nitrogen (Grachev and Severinghaus, 2003) and ΔT the temperature gradient between the top and the bottom of the firn. The depth of the firn diffusive zone is the difference between the lock-in depth (LID) at the bottom of the firn and the depth of the convective zone at the top of the firn. Previous studies based on dating constraints have shown that the existence of large convective zones at Dome C during glacial periods is highly improbable (Parrenin et al., 2012; Bazin et al., 2013; Veres et al., 2013) so that we concentrate here on the different influences on the firn LID.

The firn LID increases with increasing accumulation rate and decreases with increasing temperature (increasing metamorphism speed). On the timescale of a deglaciation, both temperature and accumulation increase so that LID is influenced by two opposite processes: LID decreases through temperature increase and LID increases through accumulation increase. In addition, it has been suggested that the concentration of impurities (taken into account through the Ca^{2+} concentration for this purpose) can increase the densification speed in the firn (Hörhold et al., 2012; Freitag et al., 2013). Since impurity concentration, as indicated by EDC calcium record (Röthlisberger et al., 2008), systematically decreases during deglaciation, it should lead to an increase of LID and hence $\delta^{15}N$. While these three effects can be accounted for in firn densification models (Freitag et al., 2013; Bréant et al.,

293 2017), reproducing the evolution of $\delta^{15}N$ over deglaciations in cold sites of East Antarctica with firn
294 densification models has long been a challenge (Sowers et al., 1992; Landais et al., 2006; Capron et al.,
295 2013; Bréant et al., 2017). In general, modeled $\delta^{15}N$ systematically decreases over terminations, while
296 ice core data indicate an increase of $\delta^{15}N$ during these periods. The temperature effect is thus
297 dominating the LID and $\delta^{15}N$ evolutions in the model at very cold sites, a feature which is not supported
298 by ice core records. In a recent firn model development (new IGE – previously LGGE – firn model), we
299 resolved the model-data mismatch by assuming that the creeping mechanism is different at very low
300 temperature (around -60°C) from the creeping mechanism at higher temperature (around -30°C)
301 (Bréant et al., 2017), a behavior supported by evidence from hot ceramic sintering (Wilkinson and
302 Ashby 1975; Bernache-Assolant, 2005).

303 Despite these firn model improvements, disentangling the effects of temperature, accumulation
304 rate and impurity concentration on the $\delta^{15}N$ evolution over deglaciations is challenging due to the
305 common co-variations of these parameters (SOM – Figure S2). Indeed, the reconstruction of snow
306 accumulation in ice cores from the East Antarctic plateau is based at first order on its relationship to
307 local temperature and inferred from water stable isotopic records (e.g. Parrenin et al., 2004). While
308 this assumption is challenged in coastal areas for centennial and millennial variability (e.g. Fudge et al.,
309 2016), the thermodynamic effect dominates at glacial to interglacial transitions. This reconstruction
310 can then be further refined using dated horizons and thinning scenarios from glaciological models as
311 done for example during the construction of the coherent ice core chronology AICC2012 (Bazin et al.,
312 2013; Veres et al., 2013). However, even with the constraints inferred from the dated horizons and
313 thinning scenarios, the accumulation rate increases significantly in parallel to δD and T_{site} over
314 deglaciations in Antarctica (SOM – Figure S2). In contrast, the link between temperature, accumulation
315 rate and Ca^{2+} is not always as strong. In particular, Termination 3 displays the strongest Ca^{2+}
316 concentration decrease observed 20 to 30 ka before the main accumulation rate and temperature
317 increase, themselves parallel to the δD signal (Figure 1, SOM – Figure S2). This makes Termination 3 a
318 unique deglaciation to disentangle the influences of impurity and temperature (accumulation).

EDC $\delta^{15}N$ increase over Termination 3 is in two steps, the first one (+ 0.06 ‰) between 256 and 248 ka and the second one (+ 0.11 ‰) between 248 and 243 ka. These increases occur more than 15 ka later than the main impurity decrease, i.e. a temporal lag much larger than the maximum 1 ka uncertainty in the relative chronology between gas age (on which $\delta^{15}N$ is displayed) and ice age (on which Ca^{2+} and δD are displayed) (Bazin et al., 2013; Veres et al., 2013). Only a small decrease in $\delta^{15}N$ (less than 0.06 ‰) is observed around 270 ka corresponding to the major Ca^{2+} concentration peak (Figure 4) with no significant changes in temperature and accumulation as inferred from the δD record. All together, these observations suggest that impurity concentration is not the major driver of the $\delta^{15}N$ evolution over Termination 3.

In order to address this result more quantitatively, we have run the IGE firn densification model equipped with impurity effect parameterization (Bréant et al., 2017) over the sequence of Termination 3 making the assumption that only impurity concentration is varying, hence keeping constant average values for temperature and accumulation rate. At EDC where the $\delta^{15}N$ record is the longest, the model produces a $\delta^{15}N$ decrease of 0.04 ‰ (compared to slightly less than 0.06 ‰ in the measurements) over the major impurity concentration peak at 270 ka. Over the Termination 3 period where the main $\delta^{15}N$ increase is observed (256 to 244 ka), the model forced by impurity concentration only simulates a + 0.03‰ $\delta^{15}N$ increase while the measured $\delta^{15}N$ increases by 0.16‰ (Figure 4). The impurity effect is hence not able to explain the $\delta^{15}N$ increase corresponding to Termination 3.

Most of the $\delta^{15}N$ increase over Termination 3 should thus be explained by changes in accumulation rate and temperature. Increase in accumulation rate leads to increases in LID and then in $\delta^{15}N$ through gravitational fractionation. At first order, the increase in $\delta^{15}N$ due to accumulation is thus expected to be parallel with the increase in δD. To check such an hypothesis, we have simulated the $\delta^{15}N$ evolution over the Termination 3 using the IGE firn densification model (Bréant et al., 2017) forced by the AICC2012-derived accumulation rate only (i.e. with constant temperature and Ca^{2+} concentration). A $\delta^{15}N$ increase of 0.103 ‰ is modelled between 253 and 243 ka (Figure 4). This change is smaller but of the same order than the 0.16 ‰ increase of measured $\delta^{15}N$. However, the modeled

345 $\delta^{15}N$ is delayed by 2 ka compared to the measured $\delta^{15}N$. This shows that an additional effect also
346 influences the $\delta^{15}N$ signal.

347 The temperature effect is more complicated to infer than the accumulation rate effect. Indeed,
348 temperature can influence the $\delta^{15}N$ evolution either through the thermal effect or through the
349 gravitational effect because of a change of the LID induced by temperature variations. The
350 temperature increase during the deglaciation leads to a decrease of the LID because of increasing firn
351 metamorphism. This effect was dominating the modeled $\delta^{15}N$ evolution in cold sites in previous firn
352 densification models. However, this effect is muted in the new version of the IGE firn densification
353 model. Running this model over Termination 3 (Figure 4) with T_{site} forcing only leads to a $\delta^{15}N$ decrease
354 of 0.058‰ between 246 and 241 ka, this decrease integrating both the thermal and the gravitational
355 effects. The thermal effect leads to a slow increase of the modeled $\delta^{15}N$ between 256 ka and 244 ka
356 (total increase of 0.044‰, Figure 4). On opposite, the gravitational effect shows a mostly late decrease
357 of 0.05 ‰ between 246-241 ka, linked to the decrease of the firn depth. Combined to a thermal $\delta^{15}N$
358 decrease between 244 and 241 ka (Figure 4), it is responsible for the global modeled $\delta^{15}N$ decrease of
359 0.058‰ between 246 and 241 ka.

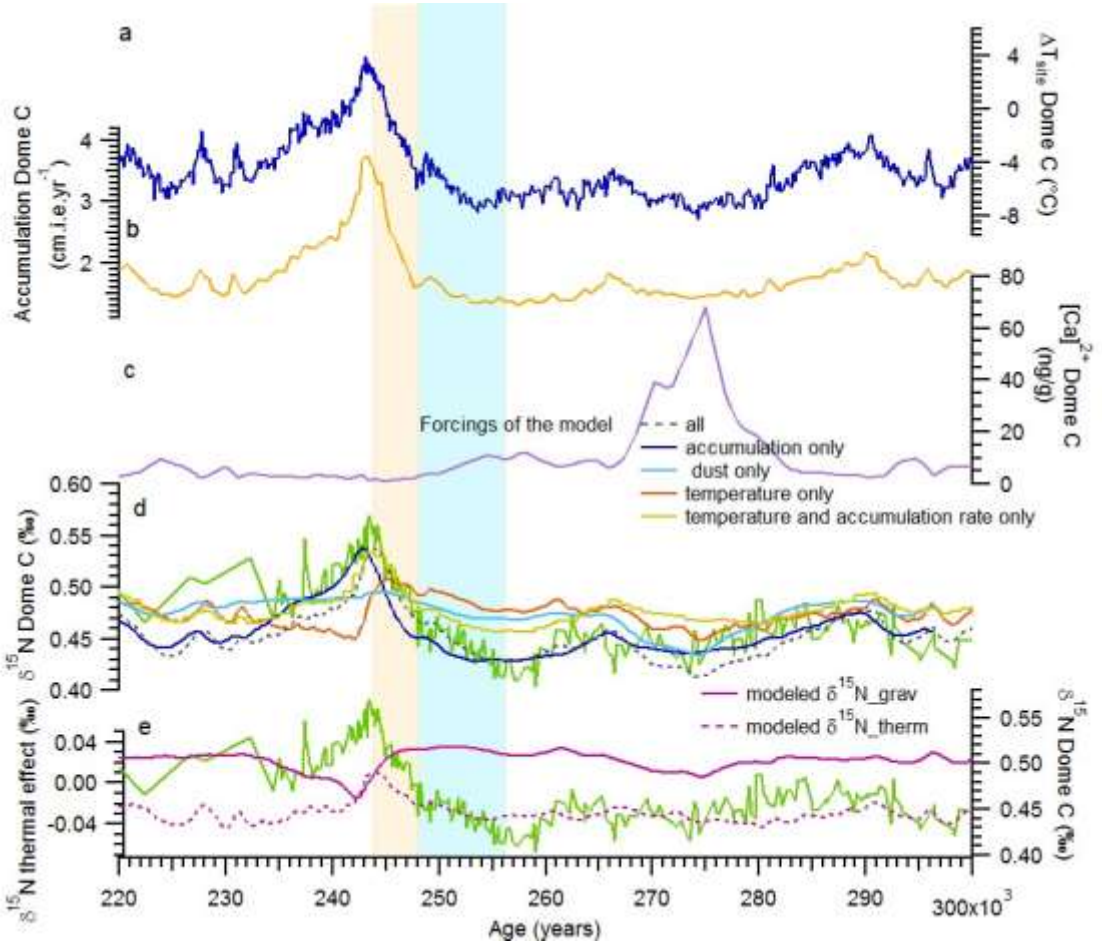

Figure 2: *Comparison between EDC $\delta^{15}N$ data with $\delta^{15}N$ simulations run with the IGE firn densification model. a: scenario for temperature forcing (difference with present-day surface temperature). b: accumulation rate scenario (from AICC2012 – the modeled $\delta^{15}N$ is not significantly modified when using the accumulation rate reconstructed from water isotopes as in Parrenin et al., 2007). c: Ca^{2+} concentration used as input scenario for the firn densification model. d: comparison of measured (green) and modelled $\delta^{15}N$ for different configurations of the IGE firn densification model (all forcing in dark blue dashed line, only accumulation forcing in dark blue, only dust forcing in light blue, only temperature forcing in red, temperature and accumulation rate forcing in yellow). e: the purple lines on the lower panel show the outputs of the IGE model forced by temperature only for both its gravitational part (solid line, right y-axis) and its thermal part (dashed line, left y-axis). The blue rectangle indicates phase 1 and the yellow rectangle indicates phase 2.*

Summarizing and based on our model-data comparison, we are now able to better explain the drivers of the $\delta^{15}N$ increase over the two increasing phases of Termination 3 (blue and yellow bars on Figure 4). During the first $\delta^{15}N$ increasing phase (blue on figure 4), the $\delta^{15}N$ increase is explained by a combination of thermal fractionation and accumulation effects, with a negligible contribution of impurity concentration. During the second $\delta^{15}N$ increasing phase (yellow on figure 4), the $\delta^{15}N$ increase is essentially driven by the increasing accumulation rate, itself mainly related to increasing temperature. The direct temperature effect plays a role in the early $\delta^{15}N$ increase over the second phase. However a few ka after the beginning of this

second $\delta^{15}N$ increasing phase, increasing thermal $\delta^{15}N$ and decreasing gravitational $\delta^{15}N$ effects compensate each other so that the total effect is nil. When taking into account the influence of temperature, accumulation rate and impurity concentration in the firn densification model as adjusted for cold and low accumulation sites of East Antarctica (Bréant et al., 2017), we observe a total modeled $\delta^{15}N$ signal in very good agreement with our data for Dome C Termination 3 as was already observed for Termination 1 (Bréant et al., 2017). This is an additional validation of the firn model development performed by Bréant et al. (2017) since the phasing between changes in temperature and changes in impurity concentrations is strongly different in Termination 1 and Termination 3. This good result can also be extended to the whole 800 ka record (SOM – Figure S3).

4- Discussion – East Antarctic climate dynamic over Termination 3

One of the characteristics of Termination 3 on the EDC δD record is the succession of two increasing phases (a first minor one followed by a larger one) between 253 and 244 ka with an interruption at 248-249 ka. The existence of these two δD increasing phases are confirmed by the $\delta^{15}N$ measurements and T_{site} reconstruction. Indeed, the $\delta^{15}N$ increase over the first phase of Termination 3 at EDC is mainly influenced by local temperature and accumulation rate, itself partly related to temperature through thermodynamic effects on multi-millennial timescale. The $\delta^{15}N$ and T_{site} data hence show that the first phase of Termination 3 is of larger amplitude than suggested by the δD record and probably started earlier (at 256 ka instead of 253 ka as suggested by the $\delta^{15}N$ signal).

4-1- Specificity of Termination 3 in other climatic records

This feature of Termination 3 is also strongly expressed in other records from relatively high latitudes of the Southern Hemisphere, such as the $\delta^{18}O_{planktonic}$ record of Pahnke et al. (2003) in the Southern Ocean, close to the east of New Zealand (Chatham Rise), reflecting either a local climatic and hydrologic modification or a front shift during the first phase of Termination 3 (Figure 5). Note that this record can be paralleled to the T_{source} reconstruction over the first phase of Termination 3 reflecting

either an increase of the oceanic temperature or a shift of the source evaporative region toward lower latitudes.

In the Northern Hemisphere, several records highlighted a succession of millennial events occurring prior to the main deglaciation signal of Termination 3 (Jiang et al., 2010; Obrochta et al., 2014; Cheng et al., 2009, 2016; Pérez-Mejías et al., 2017). The fingerprints of Heinrich-like events have been identified over this period (McManus et al., 2004), through cold periods in the Northern Atlantic (Obrochta et al., 2014), dry events in Southern Europe (Pérez-Mejías et al., 2017) and WMI in East Asian speleothems (Jiang et al., 2010; Cheng et al., 2009, 2016) (Figure 5). In particular, Cheng et al. (2009) proposed a three-phase sequence of Termination 3, the first and last phases corresponding to weak monsoon intervals. A parallel is proposed between the intermediate phase and the slight Antarctic cooling between the two Antarctic warming phases III-a and III-b displayed on Figure 2. The bipolar seesaw mechanism is expected to synchronize Greenland stadials with Southern ocean and Antarctic warming (Blunier and Brook 2001; Stocker and Johnsen 2003; EPICA Community members, 2006; Barker et al., 2009; Landais et al., 2015; Pedro et al., 2018). Within the chronological uncertainties of AICC2012 and age models of other archives (larger than 2 ka each), we follow Cheng et al. (2009) and propose that the Antarctic warming during phase III-a of Termination 3 coincides with the Heinrich-like event at 250 ka and WMI-III-a, and the Antarctic warming during phase III-b of Termination 3 corresponds to the Heinrich like event at 245 ka and WMI-III-b. To keep coherency with the notation first introduced by Cheng et al. (2009), we thus refer to T III-a and T III-b for the two Antarctic warming phases over Termination 3, these warming phases corresponding very likely to WMI III-a and WMI III-b.

4-2- <u>The sequence of Termination 3 on a coherent chronology using ice core proxies</u>

A way to circumvent the chronological issue between Antarctic records and lower latitude records and to confirm the hypothesis proposed above and by Cheng et al. (2009) is to make a direct comparison between the high latitude proxies ($\delta^{15}N$, T_{site}, δD) and low latitude proxies ($\delta^{18}O_{atm}$, CH_4 as

indirect tracers of the low latitude cycle, see below) all measured on the same EDC ice core. There is thus no relative chronology uncertainty between the records except the maximum 1 ka uncertainty (inferred from AICC2012) between records displayed on the gas timescale ($\delta^{15}N$, $\delta^{18}O_{atm}$, CH_4) and those displayed on the ice timescale (δD, T_{site}). The $\delta^{18}O_{atm}$ signal shares many similarities with East Asian $\delta^{18}O_{calcite}$ records at both orbital and millennial timescales (Wang et al., 2008; Severinghaus et al., 2009; Extier et al., 2018) because it is directly influenced by the low latitude meteoric water $\delta^{18}O$ signal transmitted to the atmosphere through photosynthesis (e.g. Bender et al., 1994; Landais et al., 2010; Seltzer et al., 2017). Moreover, Reutenauer et al. (2015) used a model approach to show that Heinrich events are associated with synchronous millennial variability of both $\delta^{18}O_{calcite}$ in East Asia and $\delta^{18}O_{atm}$. CH_4 can also provide information of low latitudes climate of the Northern Hemisphere since the main CH_4 sources are located in wetlands of the low latitudes during glacial periods (Brook et al., 2000). Still, high latitudes of the Northern Hemisphere may strongly contribute to the CH_4 atmospheric signal especially when the high latitude continental areas are free of ice in warm periods (Yu et al., 2013).

$\delta^{18}O_{atm}$ shows two increases over phases T III-a and T III-b (Figure 5). An interruption ($\delta^{18}O_{atm}$ decrease) is observed between the two phases, i.e. in phase with the slight decrease in T_{site} and $\delta^{15}N$. This interruption at ~248 ka, also observed in the $\delta^{18}O_{calcite}$ and associated with the strengthening of the East Asian Monsoon, could be linked to an Antarctic Cold Reversal as already observed over the last deglaciation (Zhang et al., 2016) and suggested by Cheng et al. (2009). The correspondence between $\delta^{15}N$ and $\delta^{18}O_{atm}$ is free from any chronological uncertainty since they are measured on exactly the same air samples. This record hence supports a synchronicity between cold events in the Northern Hemisphere (associated with Heinrich events and WMI) and warming in Antarctica over phases T III-a and T III-b.

The CH_4 record is of relatively low resolution (400 years) and probably bears a significant influence of the high latitude Northern Hemisphere during deglaciations. Still, it shows a clear increase over phase T III-a peaking at 250 ka before a low level over phase T III-b. This increase is difficult to link to a

460 warming of the high latitudes since it corresponds to a minimum of summer insolation at 65°N (despite
461 high obliquity). Another possible interpretation of this signal is to link it to millennial-scale variability.
462 A previous study performed over the last climatic cycle and last deglaciation showed that a CH_4
463 increase of several tenths of ppb is observed at the time of iceberg discharge in the North Atlantic in
464 relationship with a shift of the tropical rain belts (Rhodes et al., 2015). The occurrence of a Heinrich
465 event and associated WMI over phase T III-a may hence explain this early CH_4 peak. The main increase
466 of CH_4 then occurs at the end of phase T III-b similarly to what is observed for the other deglaciations
467 (Figures 1 and 5).

468 Our new measurements hence permit to refine the sequence of events for Termination 3
469 including Antarctica without relative chronological uncertainty. During phase T III-a occurring during a
470 minimum of the summer insolation at 65°N, Heinrich like events are associated with a southward shift
471 of the Northern Hemisphere polar front and of the tropical rain belts linked with the ITCZ (Intertropical
472 Convergence Zone). This shift is observed in the increases of $\delta^{18}O_{atm}$, East Asia $\delta^{18}O_{calcite}$ and CH_4 and is
473 associated with the weak monsoon interval referred as WMI-III-a. Connected to this Northern
474 Hemisphere change through atmospheric and oceanic teleconnections linked to the bipolar seesaw,
475 the Antarctic temperature increases as shown by the T_{site} and $\delta^{15}N$ records. Despite evidences for the
476 Northern Hemisphere vs Antarctica correspondences, our records also show that the sub-millennial
477 variability recorded in the IRD and Chinese $\delta^{18}O_{calcite}$ records over phase T III-a (2 IRD peaks, 2 positive
478 $\delta^{18}O_{calcite}$ excursions, red points in Figure 5) is not seen in the Antarctic records which record only one
479 monotonous temperature increase.

480 Phase T III-b occurs during the rise of 65°N summer insolation and is characterized by a Heinrich
481 like event of larger amplitude, which is also associated with WMI III-b, a southward shift of the ITCZ
482 and of the Northern Hemisphere polar front. In a context of high Northern Hemisphere insolation and
483 similarly to other deglaciations in the same insolation context (e.g. the most recent and well dated
484 Terminations 1 and 2, cf Figure 1), the Antarctic temperature increases faster than during phase T III-
485 a.

Finally, the sequence of events over Termination 3 can be compared with the sequences observed on Termination 1 and Termination 2 where dating constraints are strong enough (Figure 5). In particular, Figure 5 shows that we systematically have parallel increase of $\delta^{15}N$, T_{site} and T_{source} at Dome C over the one or two Antarctic warming phases of the terminations. These warming phases are also systematically associated with IRD peaks as well as increasing phases in the $\delta^{18}O_{calcite}$ and $\delta^{18}O_{atm}$. The Antarctic warmings during the last 3 deglaciations are thus systematically correlated with the occurrence of WMI and iceberg discharges in the North Atlantic, hence a southward shift of the ITCZ. However, the peculiarity of Termination III is the fact that the warming over phase T III-a occurs during a minimum in June 21st insolation at 65°N while all Antarctic warming phases occur during a phase of increase in the June 21st insolation at 65°N. This may explain why phase T III-a is associated with a much smaller δD and T_{site} increase than phase TI-a. The occurrence of phase T III-a of Termination 3 in a context of low summer insolation at 65°N hence appears as an anomaly and suggests that other factors than the increase in summer insolation in the Northern Hemisphere may play a role in the triggering of the deglaciation in Antarctica. These factors may be local insolation (i.e. Southern Hemisphere summer insolation) or occurrence of millennial scale variability related to changes in the ITCZ locations.

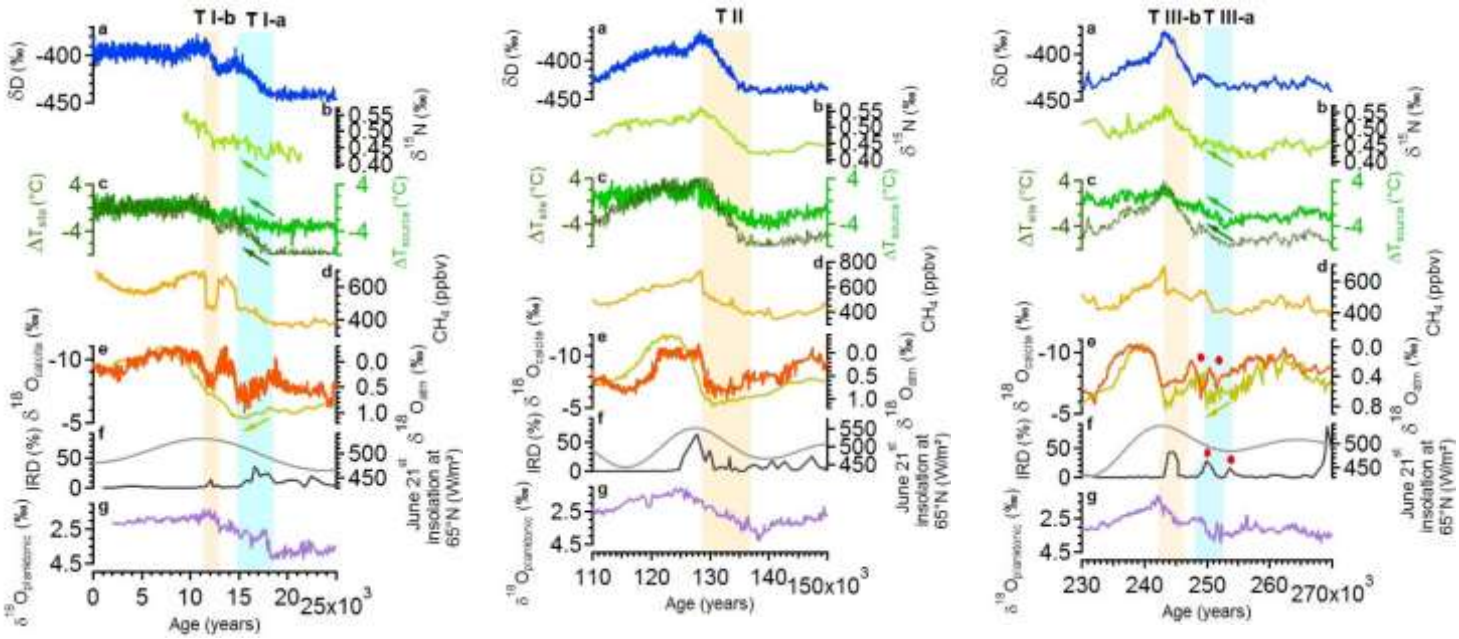

Figure 5: *Millennial variability during the Terminations 1 (left), 2 (middle) and 3 (right). a: EDC δD record (Jouzel et al., 2007). b: measured EDC $\delta^{15}N$ (Dreyfus et al., 2010; Landais et al., 2013; this study). c: EDC ΔT_{site} (dark*

green) and ΔT_{source} (green) reconstructions. d: EDC CH_4 (Loulergue et al., 2008). e: $\delta^{18}O_{calcite}$ from East Asian speleothems in red (Cheng et al., 2016) and EDC $\delta^{18}O_{atm}$ in yellow (Extier et al., 2018). f: IRD percentage from site ODP980 in black (McManus et al., 1999) and June 21st insolation at 65°N in grey (Laskar et al., 2004). g: $\delta^{18}O_{planktonic}$ of core MD97-2120 (Pahnke et al., 2003). All ice core data are presented on the AICC2012 timescale, the Δage estimate in AICC2012 between the gas and ice timescales being in excellent agreement (maximum difference of 400 years) with the Δage obtained with the IGE firnification model presented here.

5- Conclusions and perspectives

We presented a high resolution record of $\delta^{15}N$ over Termination 3 on the Dome C ice core together with a reconstruction of T_{site} and T_{source} from the combination of δD and d-excess on the same ice core. $\delta^{15}N$ and T_{site} display early increases as soon as 256 and 253 ka while the δD record is mostly stable until 251 ka. Based on a thorough data – firn model comparison, we demonstrated that impurity concentration does not influence the $\delta^{15}N$ signal over Termination 3 and that the major part of the $\delta^{15}N$ increase from 256 ka to the end of Termination 3 should better be related (directly or indirectly through accumulation) to local temperature. It follows from this multiproxy analysis that the Antarctic temperature increase over the first phase of Termination 3 is stronger than inferred from δD only.

Using a comparison with other climatic archives as well as indication for the timing of Weak Monsoon Intervals in the EDC ice core and change in the low latitude water cycle through the $\delta^{18}O_{atm}$ proxy, we confirm a sequence of events suggested by Cheng et al. (2009): the two phases of Antarctic temperature increase over Termination 3 are related to Heinrich like events with a bipolar seesaw mechanism at play. The first phase occurs during a minimum of summer Northern Hemisphere insolation with the bipolar seesaw associated with Heinrich like events being the major explanation for Antarctic temperature increase while the second phase is associated with both Heinrich like event and increase in summer Northern Hemisphere insolation. This contrasts with the two younger terminations when the first Antarctic warming phase is in phase with increased in summer insolation at 65°N.

This study confirms that using δD from the EDC ice core for reconstructing temperature evolution should be done carefully. Indeed, millennial scale events can induce synchronous cooling of source and

site temperatures resulting in a stable δD. Multiproxy studies like the one performed here are thus desirable and should be applied to other terminations such as Termination 4 associated with a strong millennial variability at the end of MIS 10. This study opens perspective for deciphering the role of orbital forcing and millennial variability in the onset and amplitude of a deglaciation.

Acknowledgments

The research leading to these results has received funding from the European Research Council under the European Union's Seventh Framework Programme (FP7/2007-2013) / RC agreement number 306045. It was also received funding from INSU/CNRS LEFE project NEVE-CLIMAT. Finally, this work is a contribution to the European Project for Ice Coring in Antarctica (EPICA).

Supplementary Online Material

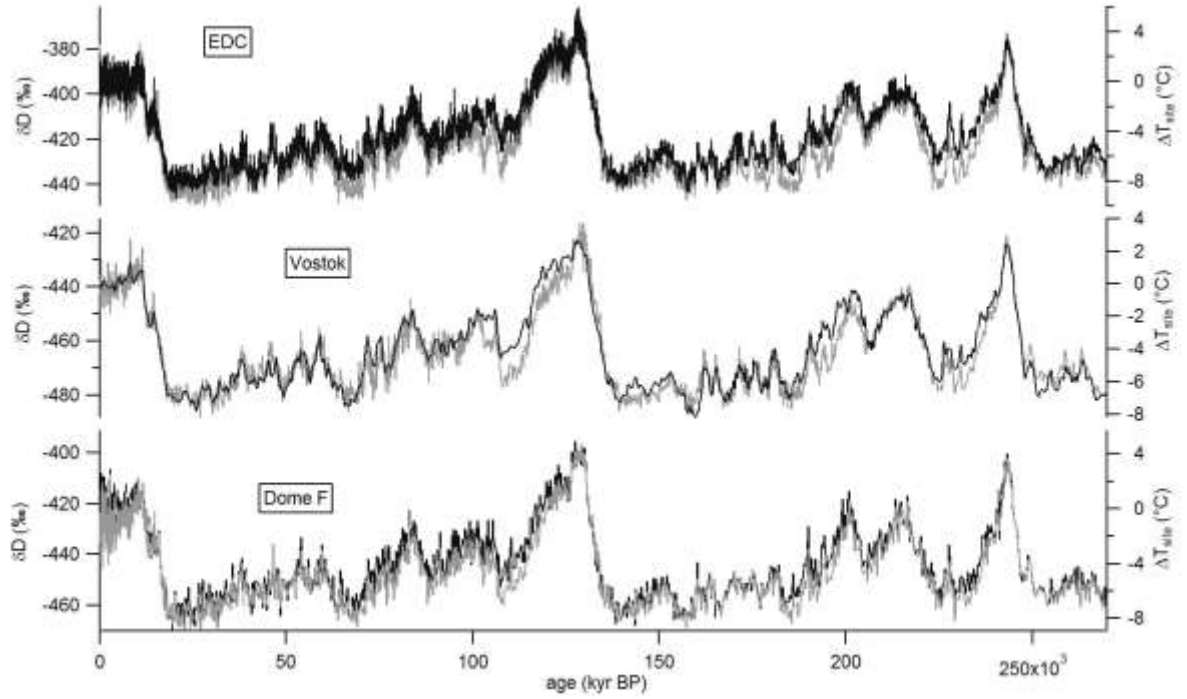

SOM - Figure S1: *Comparison of the δD (grey) and ΔT_{site} reconstructions for 3 deep ice cores in East Antarctica.*

552

553

Correlation	Dome F δD	Dome F T_{site}	EDC δD	EDC T_{site}	Vostok δD	Vostok T_{site}
Dome F δD	1	0.95	0.90	0.86	0.89	0.86
Dome F T_{site}	0.95	1	0.89	0.89	0.86	0.89
EDC δD	0.90	0.89	1	0.92	0.89	0.89
EDC T_{site}	0.86	0.89	0.92	1	0.84	0.90
Vostok δD	0.89	0.86	0.89	0.84	1	0.91
Vostok T_{site}	0.86	0.89	0.89	0.90	0.91	1

SOM - Table T1: *Correlation between δD and ΔT_{site} over the last 300 ka for Dome F, EDC and Vostok ice cores.*

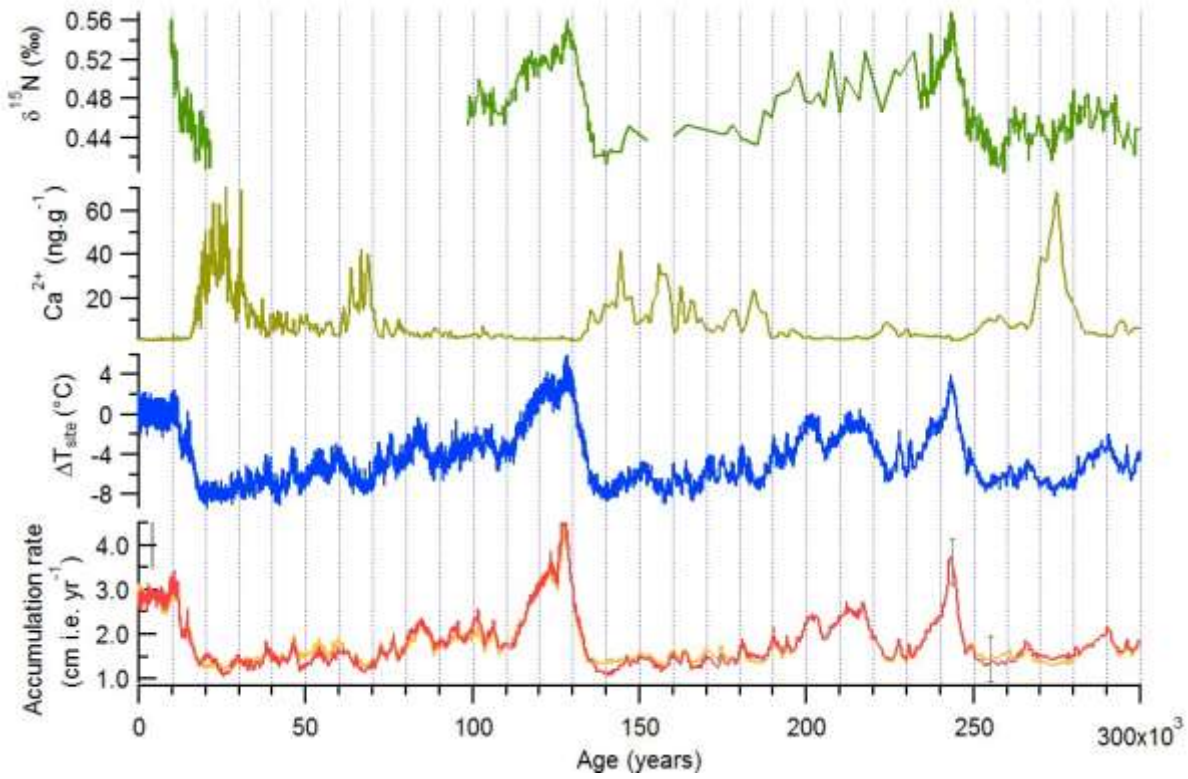

SOM - Figure S2: *Variations of $\delta^{15}N$, Ca^{2+} concentration (Lambert et al., 2012), ΔT_{site} and accumulation rate (red from water isotopes as in Parrenin et al., 2007; orange from AICC2012) on the EDC ice core. The grey error bars show the uncertainty associated with accumulation rate reconstruction in AICC2012 for the glacial and interglacial periods delimiting Termination 3.*

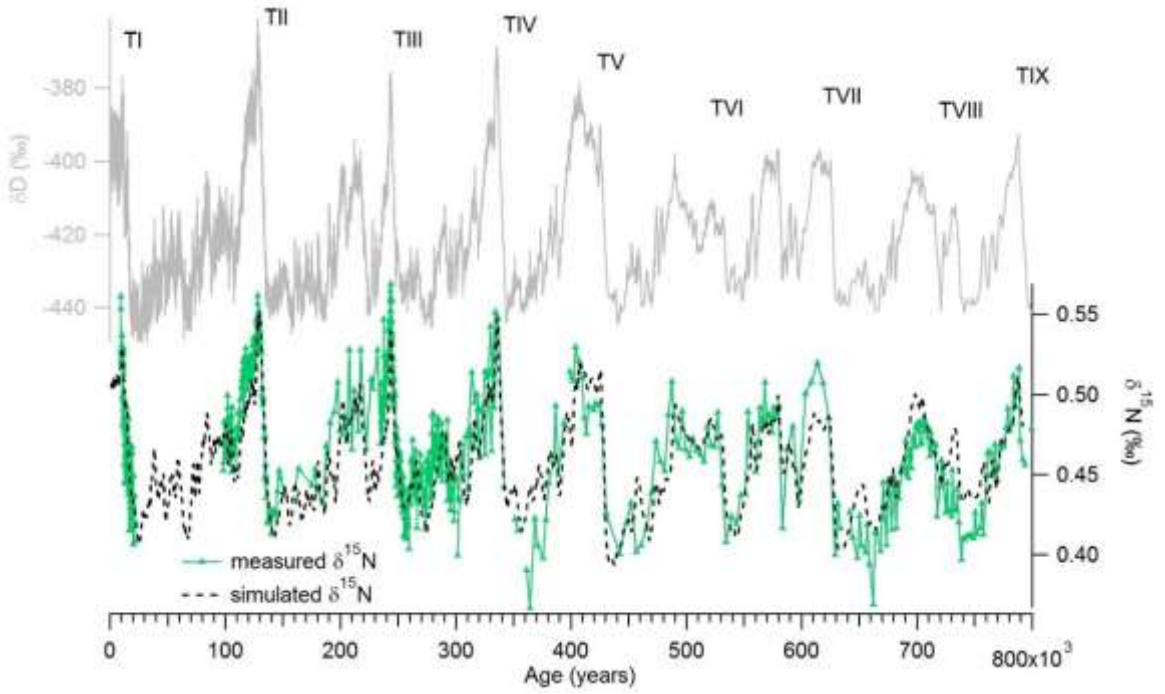

***SOM - Figure S3**: Comparison of measured (green) and modeled (IGE model of Bréant et al., 2017, including all dust, accumulation and temperature forcings, dashed black line) $\delta^{15}N$ over the last 800 ka at Dome C.*

References

Barker, S., Diz, P., Vautravers, M.J., Pike, J., Knorr, G., Hall, I.R., Broecker, W.S., 2009. Interhemispheric Atlantic seesaw response during the last deglaciation. Nature 457, 1097–1102.

Bazin, L., Landais, A., Lemieux-Dudon, B., Toyé Mahamadou Kele, H., Veres, D., Parrenin, F., Martinerie, P., Ritz, C., Capron, E., Lipenkov, V., Loutre, M.-F., Raynaud, D., Vinther, B., Svensson, A., Rasmussen, S.O., Severinghaus, M., Blunier, T., Leuenberger, M., Fischer, H., Masson-Delmotte, V., Chappellaz, J., Wolff, E., 2013. An optimized multi-proxy, multi-site Antarctic ice and gas orbital chronology (AICC2012): 120-800 ka. Clim. Past 9, 1715–1731.

Bender, M.L., Sowers, T., Labeyrie, L., 1994. The Dole effect and its variations during the last 130,000 years as measured in the Vostok ice core. Global Biogeochem. Cycles 8, 363–376.

Bereiter, B., Eggleston, S., Schmitt, J., Nehrbass-Ahles, C., Stocker, T. F., Fischer, H., Kipfstuhl, S., Chappellaz, J., 2015. Revision of the EPICA Dome C CO_2 record from 800 to 600 kyr before present. Geophysical Research Letters 42, 542–549.

Bernache-Assollant, D., 2005. Frittage : aspects physico-chimiques Partie 2 : frittage en phase liquide.

584 Bintanja, R., van de Wal, R.S.W., Oerlemans, J., 2005. Modelled atmospheric temperatures and global
585 sea levels over the past million years. Nature 437, 125–128.
586 Blunier, T. and Brook, E.J., 2001. Timing of millennial-scale climate change in Antarctica and Greenland
587 during the last glacial period. Science 291 (5501), 109–112.
588 Bréant, C., Martinerie, P., Orsi, A., Laurent, A., Landais, A., 2017. Modelling firn thickness evolution
589 during the last deglaciation: constraints on sensitivity to temperature and impurities. Clim. Past
590 13(7), 833–853.
591 Brook, E.J., Harder, S., Severinghaus, J., Steig, E.J., Sucher, C.M., 2000. On the origin and timing of rapid
592 changes in atmospheric methane during the Last Glacial Period. Global Biogeochemical Cycles 14
593 (2), 559–572.
594 Caillon, N., Severinghaus, J.P., Jouzel, J., Barnola, J.M., Kang, J., Lipenkov, V.Y., 2003. Timing of
595 atmospheric CO_2 and Antarctic temperature changes across Termination III. Science 299, 1728–
596 1731.
597 Capron, E., Landais, A., Lemieux-Dudon, B., Schilt, A., Masson-Delmotte, V., Buiron, D., Chappellaz, J.,
598 Dahl-Jensen, D., Johnsen, S., Leuenberger, M., Loulergue, L., Oerter, H., 2010. Synchronising EDML
599 and NorthGRIP ice cores using $\delta^{18}O$ of atmospheric oxygen ($\delta^{18}O_{atm}$) and CH_4 measurements over
600 MIS5 (80–123 kyr). Quat. Sci. Rev. 29, 222–234.
601 Capron, E., Landais, A., Buiron, D., Cauquoin, A., Chappellaz, J., Debret, M., Jouzel, J., Leuenberger, M.,
602 Martinerie, P., Masson- Delmotte, V., Mulvaney, R., Parrenin, F., Prié, F., 2013. Glacial–interglacial
603 dynamics of Antarctic firn columns: comparison between simulations and ice core air-$\delta^{15}N$
604 measurements. Clim. Past 9, 983–999.
605 Ciais, P. and Jouzel, J. 1994. Deuterium and oxygen 18 in precipitation: Isotopic model, including mixed
606 cloud processes. Journal of Geophysical Research: Atmospheres 99, 16793-16803
607 Cheng, H., Edwards, R. L., Broecker, W. S., Denton, G. H., Kong, X., Wang, Y., . . . Wang, X. (2009). Ice
608 Age Terminations. Science, 326(5950), 248-252. doi:10.1126/science.1177840

609 Cheng, H., Edwards, R.L., Sinha, A., Spötl, C., Yi, L., Chen, S., Kelly, M., Kathayat, G., Wang, X., Li, X.,
610 Kong, X., Wang, Y., Ning, Y., Zhang, H., 2016. The Asian monsoon over the past 640,000 years and
611 ice age terminations. Nature 534, 640–646.
612 Chiang, J.C.H., Bitz, C.M., 2005. Influence of high latitude ice cover on the marine Intertropical
613 Convergence Zone. Clim. Dyn. 25, 477–496.
614 Denton, G.H., Anderson, R.F., Toggweiler, J.R., Edwards, R.L., Schaefer, J.M., Putnam, A.E., 2010. The
615 last glacial termination. Science 328, 1652–1656.
616 Dreyfus, G.B., Jouzel, J., Bender, M.L., Landais, A., Masson-Delmotte, V., Leuenberger, M., 2010. Firn
617 processes and $\delta^{15}N$: potential for a gas-phase climate proxy. Quat. Sci. Rev. 29, 28–42.
618 Dütsch, M., Pfahl, S., Sodemann, H., 2017. The impact of nonequilibrium and equilibrium fractionation
619 on two different deuterium excess definitions. Journal of Geophysical Research: Atmospheres
620 122, 12732–12746.
621 EPICA Community Members, 2004. Eight glacial cycles from an Antarctic ice core. Nature 429, 623–
622 628.
623 EPICA Community Members, 2006. One-to-one coupling of glacial climate variability in Greenland and
624 Antarctica. Nature 444, 195–198.
625 Extier, T., Landais, A., Bréant, C., Prié, F., Bazin, L., Dreyfus, G., Roche, D.M., Leuenberger, M., 2018. On
626 the use of $\delta^{18}O_{atm}$ for ice core dating. Quat. Sci. Rev. 185, 244-257.
627 Fudge, T.J., Markle, B.R., Cuffey, K.M., Buizert, C., Taylor, K.C., Steig, E.J., Waddington, E.D., Conway,
628 H., Koutnik, M., 2016. Variable relationship between accumulation and temperature in West
629 Antarctica for the past 31,000 years. Geophys. Res. Lett. 43, 3795-3803.
630 Freitag, J., Kipfstuhl, S., Laepple, T., Wilhelms, F., 2013. Impurity-controlled densification: a new model
631 for stratified polar firn. Journal of Glaciology 59 (218), 1163–1169.
632 Gat, J.R., Matsui, E., 1991. Atmospheric water balance in the Amazon basin: an isotopic
633 evapotranspiration model. J. Geophys. Res. 96, 13179–13188.

Grachev, A.M. Severinghaus, J.P., 2003. Determining the thermal diffusion factor for Ar-40/Ar-36 in air to aid paleoreconstruction of abrupt climate change. J. Phys. Chem. 107, 4636–4642.

Hodell, D.A., Channell, J.E.T., Curtis, J.H., Romero, O.E., Röhl, U., 2008. Onset of "Hudson Strait" Heinrich events in the eastern North Atlantic at the end of the middle Pleistocene transition (~640 ka)? Paleoceanography 23, PA4218.

Hörhold, M.W., Laepple, T., Freitag, J., Bigler, M., Fischer, H., Kipfstuhl, S., 2012. On the impact of impurities on the densification of polar firn. Earth Planet. Sc. Lett. 325, 93–99.

Huybers, P., 2007. Glacial variability over the last two million years: an extended depth-derived agemodel, continuous obliquity pacing, and the Pleistocene progression. Quat. Sci. Rev. 26(1-2), 37–55.

Jiang, X., Kong, X., Wang, Y., Cheng, H., Wu, J., & Chen, S., 2010. Orbital-and millennial-scale variability of the Asian monsoon during MIS8 from Sanbao Cave at Mount Shennongjia, central China. Chinese science bulletin 55 (11), 1041–1046.

Jouzel, J., and Merlivat, L., 1984. Deuterium and oxygen-18 in precipitation: Modeling of the isotopic effects during snow formation. J. Geophys. Res. 89 (D7), 11749–11757.

Jouzel, J., Vimeux, F., Caillon, N., Delaygue, G., Hoffmann, G., Masson-Delmotte, V., Parrenin, F., 2003. Magnitude of isotope/temperature scaling for interpretation of central Antarctic ice cores. J. Geophys. Res. 108 (D12), 4361.

Jouzel, J., Masson-Delmotte, V., Cattani, O., Dreyfus, G., Falourd, S., Hoffmann, G., Minster, B., Nouet, J., Barnola, J.M., Chappellaz, J., Fischer, H., Gallet, J.C., Johnsen, S., Leuenberger, M., Loulergue, L., Luethi, D., Oerter, H., Parrenin, F., Raisbeck, G., Raynaud, D., Schilt, A., Schwander, J., Selmo, E., Souchez, R., Spahni, R., Stauffer, B., Steffensen, J.P., Stenni, B., Stocker, T.F., Tison, J.L., Werner, M., Wolff, E.W., 2007. Orbital and millennial Antarctic climate variability over the past 800,000 years. Science 317, 793–796.

Lambert, F., Bigler, M., Steffensen, J.P., Hutterli, M., Fischer, H., 2012. Centennial mineral dust variability in high-resolution ice core data from Dome C, Antarctica. Clim. Past 8, 609–623.

660 Landais, A., Barnola, J. M., Kawamura, K., Caillon, N., Delmotte, M., Van Ommen, T., Dreyfus, G., Jouzel,
661 J., Masson-Delmotte, V., Minster, B., Freitag, J., Leuenberger, M., Schwander, J., Huber, C.,
662 Etheridge, D., Morgan, V., 2006. Firn-air $\delta^{15}N$ in modern polar sites and glacial–interglacial ice: a
663 model-data mismatch during glacial periods in Antarctica? Quat. Sci. Rev. 25, 49–62.
664 Landais, A., Dreyfus, G., Capron, E., Masson-Delmotte, V., Sanchez-Goñi, M.F., Desprat, S., Hoffmann,
665 G., Jouzel, J., Leuenberger, M., Johnsen, S., 2010. What drives the millennial and orbital variations
666 of $\delta^{18}O_{atm}$? Quat. Sci. Rev. 29, 235–246.
667 Landais, A., Dreyfus, G., Capron, E., Jouzel, J., Masson-Delmotte, V., Roche, D.M., Prié, F., Caillon, N.,
668 Chappellaz, J., Leuenberger, M., Lourantou, A., Parrenin, F., Raynaud, D., Teste, G., 2013. Two-
669 phase change in CO_2, Antarctic temperature and global climate during Termination II. Nat. Geosci.
670 6, 1062–1065.
671 Landais, A., Masson-Delmotte, V., Stenni, B., Selmo, E., Roche, D.M., Jouzel, J., Lambert, F., Guillevic,
672 M., Bazin, L., Arzel, O., Vinther, B., Gkinis, V., Popp, T., 2015. A review of the bipolar seesaw from
673 synchronized and high resolution ice core water stable isotope records from Greenland and East
674 Antarctica. Quat. Sci. Rev. 114, 18–32.
675 Laskar, J., Robutel, P., Joutel, F., Gastineau, M., Correia, A.C.M., Levrard, B., 2004. A long-term
676 numerical solution for the insolation quantities of the Earth. Astron. Astrophys 428, 261–285.
677 Loulergue, L., Schilt, A., Spahni, R., Masson-Delmotte, V., Blunier, T., Lemieux, B., Barnola, J.-M.,
678 Raynaud, D., Stocker, T.F., Chappellaz, J., 2008. Orbital and millennial-scale features of
679 atmospheric CH_4 over the past 800,000 years. Nature 453, 383–386.
680 Lüthi, D., Le Floch, M., Bereiter, B., Blunier, T., Barnola, J.-M., Siegenthaler, U., Raynaud, D., Jouzel, J.,
681 Fischer, H., Kawamura, K., Stocker, T.F., 2008. High-resolution carbon dioxide concentration
682 record 650,000–800,000 years before present. Nature 453, 379–382.
683 Markle, B.R., Steig, E.J., Buizert, C., Schoenemann, S.W., Bitz, C.M., Fudge, T.J., Pedro, J.B., Ding, Q.,
684 Jones, T.R., White, J.W.C, Todd, S., 2016. Global atmospheric teleconnections during Dansgaard-
685 Oeschger events. Nat. Geosci. 10, 36–40.

686 Masson-Delmotte, V., Stenni, B., Blunier, T., Cattani, O., Chappellaz, J., Cheng, H., Dreyfus, G.,
687 Edwards, R. L., Falourd, S., Govin, A., Kawamura, K., Johnsen, S. J., Jouzel, J., Landais, A., Lemieux-
688 Dudon, B., Lourantou, A., Marshall, G., Minster, B., Mudelsee, M., Pol, K., Röthlisberger, R., Selmo,
689 E., Waelbroeck, C., 2010. Abrupt change of Antarctic moisture origin at the end of Termination II.
690 P. Natl. Acad. Sci. USA, 107, 12091–12094.
691 McManus, J.F., Oppo, D.W., Cullen, J.L., 1999. A 0.5 million-year record of millennial scale climate
692 variability in the North Atlantic. Science 283, 971–975.
693 McManus, J.F., Francois, R., Gherardi, J.M., Keigwin, L.D., Brown-Leger, S., 2004. Collapse and rapid
694 resumption of Atlantic meridional circulation linked to deglacial climate changes. Nature 428,
695 834–837.
696 Merlivat L. and Jouzel J., 1979. Global climatic interpretation of the deuterium-oxygen–18 relationship
697 or precipitation. J. Geophys. Res. 84, 5029–5033.
698 Meyer, H., Schönicke, L., Wand, U., Hubberten, H.-W., Friedrichsen, H., 2000. Isotope studies of
699 hydrogen and oxygen in ground ice-experiences with the equilibration technique. Isot. Environ.
700 Health Stud. 36 (2), 133–149.
701 Milankovitch, M., 1941. History of radiation on the Earth and its use for the problem of the ice ages. K.
702 Serb. Akad. Beogr.
703 Obrochta, S.P., Crowley, T.J., Channell, J.E., Hodell, D.A., Baker, P.A., Seki, A., Yokoyama, Y., 2014.
704 Climate variability and ice-sheet dynamics during the last three glaciations. Earth and Planetary
705 Science Letters 406, 198–212.
706 Past Interglacials Working Group of PAGES, 2016. Interglacials of the last 800,000 years. Reviews of
707 Geophysics 54, 162–219.
708 Pahnke, K., Zahn, R., Elderfield, H., Schulz, M., 2003. 340,000 year centennial-scale marine record of
709 Southern Hemisphere climatic oscillation. Science 301, 948–952.
710 Paillard, D., 1998. The timing of Pleistocene glaciations from a simple multiple-state climate model.
711 Nature 391, 378–381.

712 Paillard, D., Parrenin, F., 2004. The Antarctic ice sheet and the triggering of deglaciations. Earth and
713 Planetary Science Letters 227, 263–271.
714 Parrenin, F., Remy, F., Ritz, C., Siegert, M., Jouzel, J., 2004. New modelling of the Vostok ice flow
715 line and implication for the glaciological chronology of the Vostok ice core. J. Geophys. Res.,
716 109, D20102.
717 Parrenin, F., Barnola, J.-M., Beer, J., Blunier, T., Castellano, E., Chappellaz, J., Dreyfus, G., Fischer, H.,
718 Fujita, S., Jouzel, J., Kawamura, K., Lemieux-Dudon, B., Loulergue, L., Masson-Delmotte, V., Narcisi,
719 B., Petit, J.-R., Raisbeck, G., Raynaud, D., Ruth, U., Schwander, J., Severi, M., Spahni, R., Steffensen,
720 J. P., Svensson, A., Udisti, R., Waelbroeck, C., Wolff, E., 2007.The EDC3 chronology for the EPICA
721 Dome C ice core. Clim. Past 3, 485–497.
722 Parrenin, F., Barker, S., Blunier, T., Chappellaz, J., Jouzel, J., Landais, A., Masson-Delmotte, V.,
723 Schwander, J., Veres, D., 2012. On the gas-ice depth difference (Δdepth) along the EPICA Dome C
724 ice core. Clim. Past 8, 1239–1255.
725 Parrenin, F., Masson-Delmotte, V., Kohler, P., Raynaud, D., Paillard, D., Schwander, J., Barbante, C.,
726 Landais, A., Wegner, A., Jouzel, J., 2013. Synchronous Change of Atmospheric CO_2 and Antarctic
727 Temperature During the Last Deglacial Warming. Science 339, 1060–1063.
728 Pedro, J.B., Rasmussen, S.O., van Ommen, T.D., 2012. Tightened constraints on the time-lag between
729 Antarctic temperature and CO_2 during the last deglaciation. Clim. Past 8, 1213–1221.
730 Pedro, J.B., Jochum, M., Buizert, C., He, F., Barker, S., Rasmussen, S.O., 2018. Beyond the bipolar
731 seesaw: toward a process understanding of interhemispheric coupling. Quat. Sci. Rev. 192, 27–
732 46.
733 Pérez-Mejías, C., Moreno, A., Sancho, C., Bartolomé, M., Stoll, H., Cacho, I., Cheng, H., Edwards, R.L.,
734 2017. Abrupt climate changes during Termination III in Southern Europe. Proceedings of the
735 National Academy of Sciences 114, 10047–10052.

Reutenauer, C., Landais, A., Blunier, T., Bréant, C., Kageyama, M., Woillez, M.-N., Risi, C., Mariotti, V., Braconnot, P., 2015. Quantifying molecular oxygen isotope variations during a Heinrich stadial. Clim. Past 11, 1527–1551.

Rhodes, R.H., Brook, E.J., Chiang J., Blunier, T., Maselli, O., McConnel, J.R., Romanini, D., Severinghaus, J., 2015. Enhanced tropical methane production in response to iceberg discharge in the North Atlantic. Science 348 (6238), 1016–1019.

Röhling, E.J., Foster, G.L., Grant, K.M., Marino, G., Roberts, A.P., Tamisiea, M.E., Williams, F., 2014. Sea-level and deep-sea-temperature variability over the past 5.3 million years. Nature 508, 477–482.

Röthlisberger, R., Mudelsee, M., Bigler, M., de Angelis, M., Fisher, H., Hansson, M., Lambert, F., Masson-Delmotte, V., Sime, L., Udisti, R., Wolff, E.W., 2008. The Southern Hemisphere at glacial terminations: insights from the Dome C ice core. Clim. Past 4, 345–356.

Seltzer, A.M., Buizert, C., Baggenstos, D., Brook, E.J., Ahn, J., Yang, J.-W., Severinghaus, J.P., 2017. Does d18O of O2 record meridional shifts in tropical rainfall? Clim. Past 13, 1323–1338.

Severinghaus, J.P., Sowerst, T. & Alleyt, R.B., 1998. Timing of abrupt climate change at the end of the Younger Dryas interval from thermally fractionated gases in polar ice. Nature 39, 141–146.

Severinghaus, J.P., Beaudette, R., Headly, M.A., Taylor, K., Brook, E.J., 2009. Oxygen-18 of O_2 records the impact of abrupt climate change on the terrestrial biosphere. Science 324, 1431–1434.

Sowers, T., Bender, M.L., Raynaud, D., Korotkevich, Y.S., 1992. ^{15}N of N_2 in air trapped in polar ice: a tracer of gas transport in the firn and a possible constraint on ice age–gas age differences. Journal of Geophysical Research 97, 15,683–15,697.

Spratt, R.M., & Lisiecki, L.E., 2016. A Late Pleistocene sea level stack. Clim. Past 12, 1079–1092.

Stenni, B., Masson-Delmotte, V., Johnsen, S., Jouzel, J., Longinelli, A., Monnin, E., Röthlisberger, R., Selmo, E., 2001. An oceanic cold reversal during the last deglaciation. Science 293, 2074–2077.

Stenni, B., Masson-Delmotte, V., Selmo, E., Oerter, H., Meyer, H., Röthlisberger, R., Jouzel, J., Cattani, O., Falourd, S., Fisher, H., Hoffmann, G., Lacumin, P., Johnsen, S.J., Minster, B., Udisti, R., 2010.

761 The deuterium excess records of EPICA Dome C and Maud Land ice cores (East Antarctica). Quat.
762 Sci. Rev. 29, 146–159.
763 Stocker, T.F., Johnsen, S.J., 2003. A minimum thermodynamic model for the bipolar seesaw.
764 Paleoceanography 18, 1087.
765 Touzeau, A., Landais, A., Stenni, B., Uemura, R., Fukui, K., Fujita, S., 2016. Acquisition of isotopic
766 composition for surface snow in East Antarctica and the links to climatic parameters. Cryosphere,
767 10 (2), 837–852.
768 Tzedakis, P.C., Crucifix, M., Mitsui, T., & Wolff, E.W., 2017. A simple rule to determine which insolation
769 cycles lead to interglacials. Nature 542, 427–432.
770 Uemura, R., Masson-Delmotte, V., Jouzel, J., Landais, A., Motoyama, H., Stenni, B., 2012. Ranges of
771 moisture-source temperature estimated from Antarctic ice cores stable isotope records over
772 glacial–interglacial cycles. Clim. Past 8 (3), 1109–1125.
773 Uemura, R., Motoyama, H., Masson-Delmotte, V., Jouzel, J., Kawamura, K., Goto-Azuma, K., Fujita, S.,
774 Kuramoto, T., Hirabayashi, M., Miyake, T., Ohno, H., Abe-Ouchi, A., Iizuka, Y., Horikawa, S.,
775 Igarashi, M., Suzuki, K., Suzuki, T., Fujii, Y., 2018. Asynchrony between Antarctic temperature and
776 CO_2 associated with obliquity over the past 720,000 years. Nat. Comm. 9 (961).
777 Veres, D., Bazin, L., Landais, A., Toyé Mahamadou Kele, H., Lemieux-Dudon, B., Parrenin, F., Martinerie,
778 P., Blayo, E., Blunier, T., Capron, E., Chappellaz, J., Rasmussen, S.O., Severi, M., Svensson, A.,
779 Vinther, B., Wolff, E.W., 2013. The Antarctic ice core chronology (AICC2012): an optimized multi-
780 parameter and multi-site dating approach for the last 120 thousand years. Clim. Past 9, 1733–
781 1748.
782 Vimeux, F., Masson, V., Jouzel, J., Stievenard, M., Petit, J.R., 1999. Glacial–interglacial changes in ocean
783 surface conditions in the Southern Hemisphere. Nature 398, 410–413.
784 Vimeux, F., Masson, V., Jouzel, J., Petit, J.R., Steig, E.J., Stievenard, M., Vaikmae, R., White, J.W.C., 2001.
785 Holocene hydrological cycle changes in the southern hemisphere documented in East Antarctic
786 deuterium excess records. Clim. Dyn. 17, 503–513.

787 Wang, Y.J., Cheng, H., Edwards, R.L., Kong, X., Shao, X., Chen, S., Wu, J., Jiang, X., Wang, X., An, Z., 2008.
788 Millennial- and orbital-scale changes in the East Asian monsoon over the past 224,000 years.
789 Nature 451, 1090–1093.
790 Watanabe, O., Jouzel, J., Johnsen, S., Parrenin, F., Shoji, H., Yoshida, N., 2003. Homogeneous climate
791 variability across East Antarctica over the past three glacial cycles. Nature 422, 509–512.
792 Wilkinson, D.S. and Ashby, M.F., 1975. Pressure sintering by power law creep. Acta Metall. 23, 1277–
793 1285.
794 Wolff, E.W., Fischer, H., Rothlisberger, R., 2009. Glacial terminations as southern warmings without
795 northern control. Nature Geoscience 2, 206–209.
796 Yin, Q. Z. and Berger, A., 2012. Individual contribution of insolation and CO_2 to the interglacial climates
797 of the past 800,000 years. Clim. Dyn. 38, 709–724.
798 Yu, Z., Loisel, J., Turetsky, M.R., Cai, S., Zhao, Y., Frolking, S., MacDonald, G.M., Bubier, J.L., 2013.
799 Evidence for elevated emissions from high-latitude wetlands contributing to high atmospheric CH_4
800 concentration in the early Holocene. Global Biogeochem. Cycles 27, 131–140.
801 Zhang, H., Griffiths, M.L., Huang, J., Cai, Y., Wang, C., Zhang, F., Cheng, H., Ning, Y., Hu, C., Xie, S., 2016.
802 Antarctic link with East Asian summer monsoon variability during the Heinrich Stadial–Bølling
803 interstadial transition. Earth Planet. Sci. Lett. 453, 243-251.